Electronic Supplementary Material (ESI) for Soft Matter.

Supporting Information

Influence of Molecular Weight between Crosslinks on the Mechanical Properties of Polymers formed via Ring-Opening Metathesis

Tyler R. Long, Robert M. Elder, Erich D. Bain, Kevin A. Masser, Timothy W. Sirk, Jian H. Yu, Daniel B. Knorr Jr.*, Joseph L. Lenhart*

U.S. Army Research Laboratory,
Aberdeen Proving Ground, MD 21005, USA

*Corresponding authors: Daniel B. Knorr Jr., daniel.b.knorr.civ@mail.mil
Joseph L. Lenhart, joseph.l.lenhart.civ@mail.mil

Synthesis of crosslinker (HDMN)

Dicyclopentadiene (75.0 g, 0.57mol), dicyclo[2.2.1]hepta-2,5-diene (104.5 g, 1.14mol), and hydroquinone (156 mg, 1.4 mmol) were add to a glass pressure reactor. The pressure reactor was sealed and heated to 190 °C for 19h with magnetic stirring. The resulting solution was purified using fractional vacuum distillation to give a mixture of endo-endo and exo-endo products. ^{1}H NMR showed that the mixture contained 82% exo-endo product, which matched previously reported NMR data.[1] The synthesis of the HDMN produced a mixture of isomers. Both isomers are capable of creating a crosslink site during the polymerization, so the mixture was used. HDMN was chosen because it does not have any heteroatoms or space between the norbornene groups, and should behave in a manner similar to crosslinked DCPD.

Synthesis of 100000/1 ROMP Formulations

For the 100000/1 monomer to catalyst case, 3 mol % of ENB was added to DCPD to ensure it remained a liquid at room temperature. Triphenylphosphine (1.310 g, 5 mmol) was dissolved in the monomer mixture, then a 100 mg/mL solution of Grubb's 2nd generation catalyst in 1,2-dichloroethane was made. Then, 0.212 mL of the Grubb's solution (21.2 mg, 0.025 mmol of Grubb's catalyst) was added to the monomer solution, which was at room temperature. The solution was stirred for about 30 seconds before pouring the mixture into the steel mold and curing under flowing N_2 for 2 hours at 50 °C followed by post cure for 1 hour at 140 °C.

Error in $M_{c,a}$ Measurements

The degree of error in the M_c measurements was determined by comparing several batches of pDCPD that had a monomer to catalyst ratio of 5000/1 and were post cured at 175 °C. The data in Table S1 show the batch to batch variation of pDCPD, which was due to both the sensitivity of the measurement and small variations in the polymerization. The error in the M_c was also calculated by means of root mean square (RMS) error propagation from all of the relevant measurements, which is also shown in Table S1. The standard deviation achieved when comparing the different batches of pDCPD was used instead of the RMS calculation because it takes into account the batch to batch variation.

Table S1. DMA, pycnometer, and TMA results used to calculate M_c for 6 batches of pDCPD.

Batch Number	Tg (°C)	E' at 25°C (MPa)	E' at Tg-75°C (MPa)	E' min (MPa)	Density at RT (g/cm^3)	Density at E' min (g/cm^3)	M_c (g/mol)	M_c RMS (g/mol)
1	143	1820	1659	19.4	1.055	0.990	596	36
2	144	1774	1616	17.1	1.057	0.995	665	45
3	143	1806	1647	22.7	1.057	0.985	508	28
4	143	1690	1541	18.5	1.058	0.999	609	39
5	145	1702	1573	18.6	1.044	0.984	597	38
6	146	1871	1701	18.1	1.049	0.992	621	40
Average	144	1777	1623	19.1	1.053	0.991	599	38
STDEV	1	64	54	1.8	0.005	0.005	47	5

Discussion of Attempts to Control $M_{c,a}$

We first changed the crosslink density of pDCPD (decrease the $M_{c,a}$) by controlling the post cure temperature. Our standard polymerization of pDCPD was done with a 5000/1 monomer to catalyst ratio followed by curing at 50 °C for two hours then post curing at 175 °C for two hours, resulting in a T_g of 145 °C ± 2 °C. A series of pDCPD samples were synthesized with higher post cure temperatures ranging from 200 °C to 250 °C. Increasing the post cure temperature decreased the $M_{c,a}$ from 588 to 343, but this was a small range and showed no statistically-significant effect on the normalized KE_{50}, which ranged from 3.35 ± 0.18 to 3.20 ± 0.13 (Figure S1A). The change in $M_{c,a}$ could be the result of increased mobility of the Grubbs catalyst when the polymer was heated well above 145 °C, i.e., above the T_g of our standard 5000/1 pDCPD formulation and curing procedure. The increase in crosslink density also resulted in an increase in T_g to 165 °C for the pDCPD post cured to 250 °C.

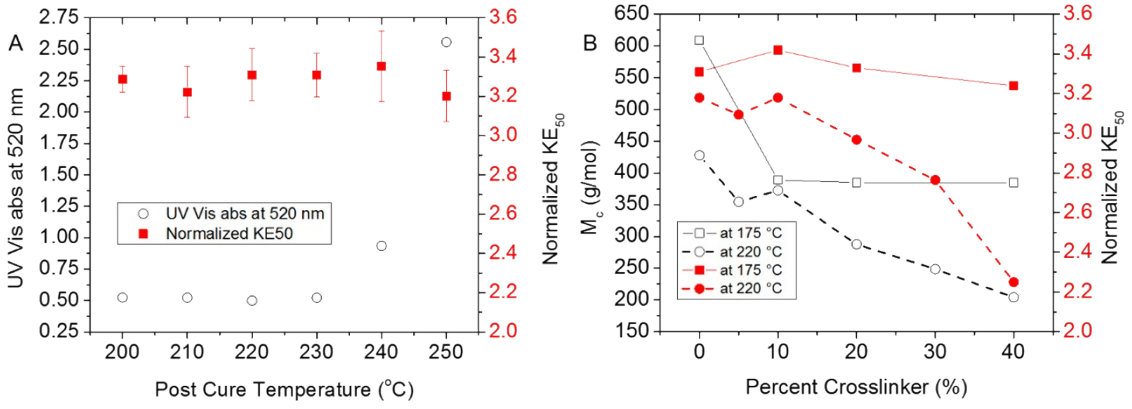

Figure S1. (A) UV-vis absorption and KE_{50} results for pDCPD resins cured at high temperatures. (B) The HDMN concentration effect on the $M_{c,a}$ (open white symbols) and normalized KE_{50} (closed red symbols) at a 5000/1 monomer to catalyst loading and a post cure temperature of 175 °C (solid line) and at a 3000/1 monomer to catalyst loading and a post cure temperature of 220 °C (dashed line).

Alternatively, the resin crosslink density may have increased with post cure temperature due to free radical generation. This is supported by the observed discoloration of the materials at elevated post cure temperatures. The discoloration of pDCPD at different post cure temperatures was characterized by UV-Vis spectroscopy. The absorption at 520 nm of a 6 mm thick sample shows that the pDCPD became discolored at post cure temperatures between 230 °C and 240 °C (Figure S1A). Due to the lack of control over the crosslinking/oxidation of these materials at elevated temperatures, simply increasing the post cure temperature is not an ideal mechanism for controlling properties. To address this issue, we synthesized a crosslinking monomer, HDMN, to precisely control the crosslink density without inducing oxidation/discoloration.

A series of copolymers were fabricated with 10, 20, and 40 mol % of HDMN in DCPD using a 5000/1 monomer to catalyst ratio and a post cure temperature of 175 °C. The $M_{c,a}$ initially decreased from 518 g/mol to 338 g/mol with the addition of 10 mol % HDMN, but when more HDMN was added (20% and 40%) there was not a significant drop in the $M_{c,a}$ (Figure S1B). These HDMN/DCPD copolymers at 10, 20, and 40 mol% HDMN all have a T_g of around 160 °C. We believe that the plateau in the $M_{c,a}$ is due to a decrease in catalyst mobility as the T_g approached the post cure temperature of 175 °C, which may have limited the crosslink density. To further reduce $M_{c,a}$, the monomer to catalyst ratio was reduced to 3000/1, and the post cure temperature was increased to 220 °C. These adjustments allowed us to systematically increase the crosslink density by increasing the HDMN concentration (Figure S1B).

Figure S1B also shows the effect of crosslinker concentration on the KE_{50}. As shown, the KE_{50} values of the polymers cured using a catalyst ratio of 5000/1 did not change more than a standard deviation, but the KE_{50} values for the polymers cured using a 3000/1 ratio decrased significantly with increasing crosslinker concetration. It is also interesting that the KE_{50} data for the 3000/1 ratio are all lower that those of the 5000/1, even for the pDCPD without crosslinker.

Fox-Flory for pDCPD/ENB

Figure S2 provides T_g data for the DCPD/ENB mixtures, and demonstrates good agreement with the Fox-Flory prediction for blend T_g values. This was not performed for HDMN as there was no “pure” HDNM formulation for comparison.

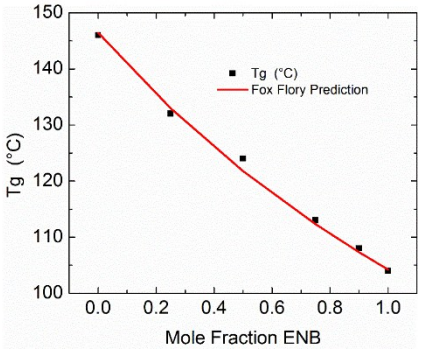

Figure S2. Change in T_g with change in mole fraction of ENB fitted to the Fox-Flory equation.

Relationship between temperature, yield stress, and fracture toughness

Figure S3A plots the data from Figure 5D as a function of measurement temperature T rather than T-T_g. The approximately linear variation in yield stress σ_y with measurement temperature T for samples at constant T-T_g = -75°C (blue diamonds) emphasizes the point made in the paper, that shifts in T- T_g as a function of M_c are not alone sufficient to explain the variations in yield stress, as is commonly assumed in the literature for glassy networks. Figure S3B shows fracture toughness K_{IC} as a function of σ_y for both ROMP series as well as several literature reports for epoxy networks. At room temperature the ROMP data follow the general trend seen for epoxies of increasing K_{IC} with decreasing σ_y, consistent with the common hypothesis that energy dissipation in the crack tip plastic zone is highly dependent on the accessibility of plastic deformation processes. However, ROMP networks tested at constant T-T_g = -75°C follow the opposite trend, with systematically increasing K_{IC} as a function of σ_y. This trend requires more research to explain fully, but may represent a transition in the mechanism(s) of yielding with increasing measurement temperature at constant T-T_g, which could also be related to the complex temperature dependence of σ_y discussed above and in the paper.

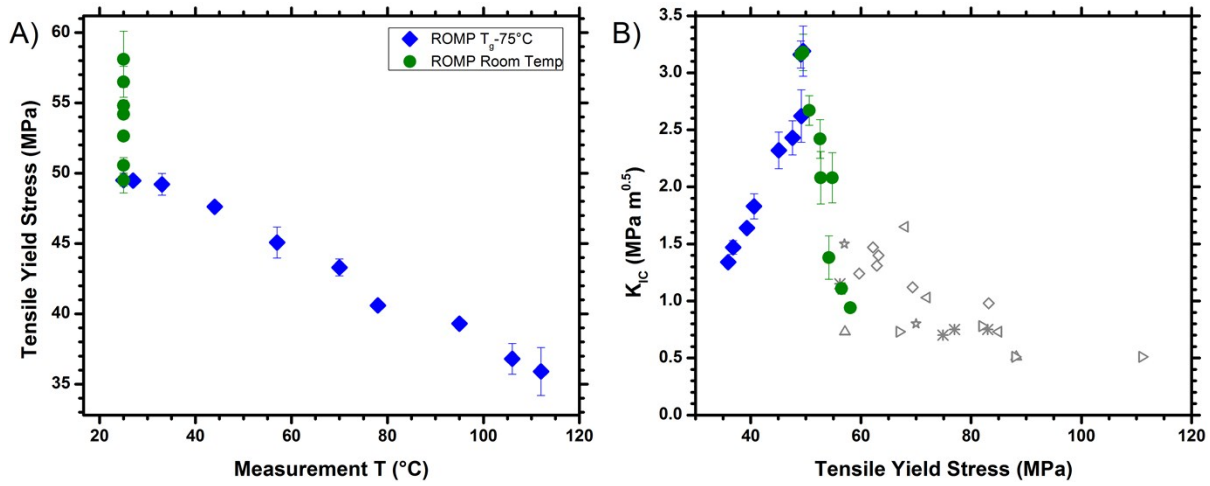

Figure S3. A) Change in yield stress as a function of measurement temperature for ROMP resins at room temperature and T = T_g-75°C. B) Comparison of fracture toughness K_{IC} as a function of tensile yield stress for ROMP resins at room temperature and T = T_g-75°C to epoxy network data from the literature: ✳[2], Δ[3], ▷[4], ◁[5], ◊[6], ★[7] (symbols refer to the same references as Figure 5 in the paper).

Modes of Failure during High Rate Testing

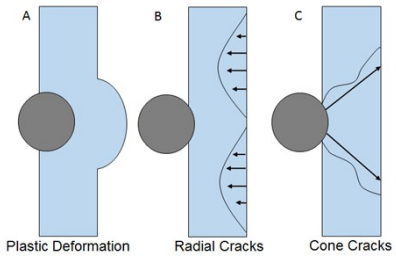

Figure S4. Three types of damage that are observed during a high rate impact test.

Images of High Rate Specimens

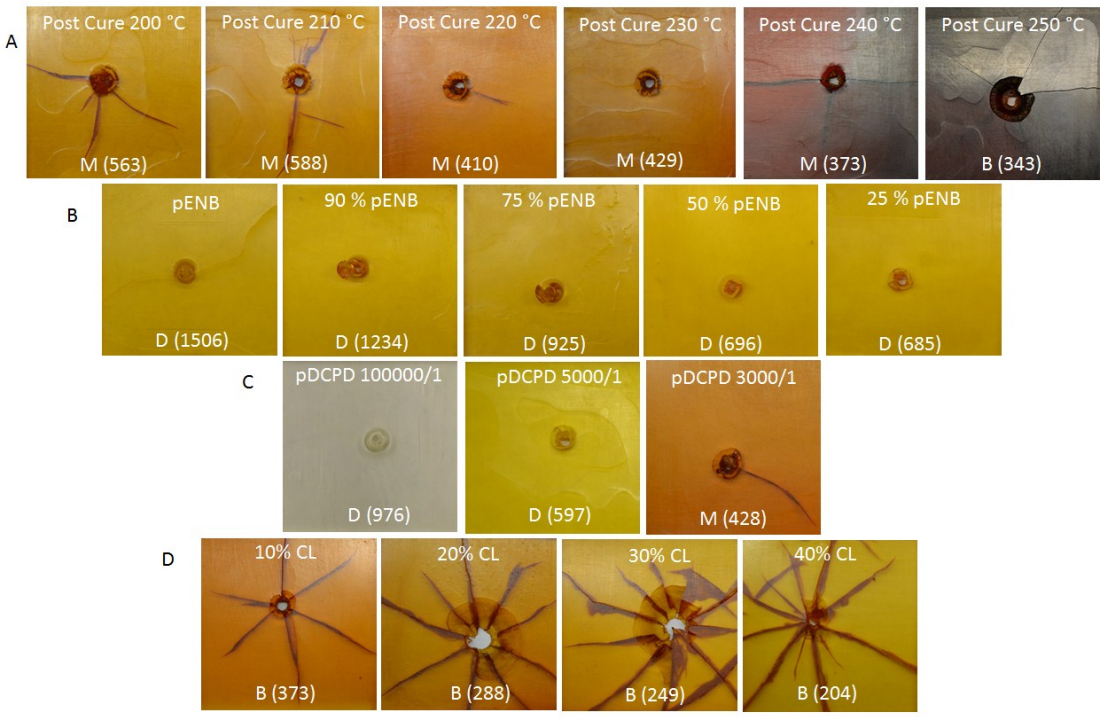

Figure S5. Photos of high rate samples for A) the pDCPD post-cured at higher temperatures, B) the series ENB/DCPD copolymers post-cured at 175°C and a 5000/1 catalyst loading, C) pDCPD cured with at different catalyst loading and post cured temperature, and D) the series of HDMN/DCPD copolymers post-cured at 220°C and a 3000/1 catalyst loading. Each polymer is denoted with the $M_{c,a}$ in g/mol.

Comparison of ROMP and Epoxy High Rate Failure

The room temperature KE_{50} of the polymers that showed more ductile failure mechanisms (ENB/DCPD copolymers) were compared to epoxy resins that have a similar T_g. As shown in Figure S6, the ENB/DCPD copolymers have up to 4-fold greater high rate impact resistance than the epoxy resins. Furthermore, epoxies also have a brittle failure mechanism over the whole range of T_g from 100 to 178°C, as can be seen in Figure S6, whereas pDCPD 5000/1 is entirely ductile with a T_g of 145°C. The high T_g, very high $KE_{50,}$ and ductile failure mechanism of ENB/DCPD copolymers make them attractive as replacements for epoxy resins.

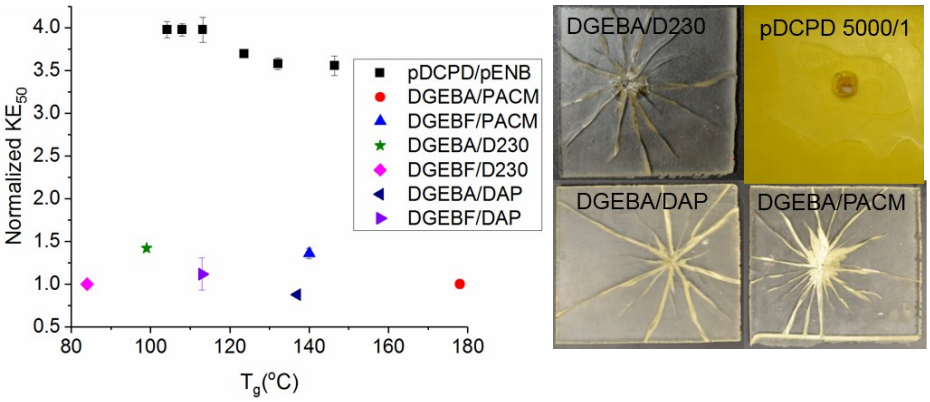

Figure S6. Comparison of the normalized KE_{50} of pDCPD/ENB copolymers with amine cured epoxy system with similar T_g values with specimens of samples tested at KE_{50} Showing extensive cracking. Here, DGEBA is diglycidyl ether of bisphenol A, while DGEBF is diglycidyl ether of bisphenol F. PACM is 4,4'-methylenebis(cyclohexylamine), D230 is a Huntsman Jeffamine® product and DAP is 1,3-diaminopropane.

Molecular Dynamics Simulation Change in Volume for pDCPD and pENB

In our simulations, pENB has lower density than linear pDCPD (0.94 vs. 1.03 g cm^{-3} at 300 K, which is in reasonable agreement with the data in Table S1 at ~298K), and higher volumetric expansion during deformation (Figure S6), while also having identical nanovoid volume percent (Figure 9 in the text). These results indicate that pENB has a greater amount of molecular-scale interstitial space than linear pDCPD. This is consistent with the experimental observations of volume expansion at larger scales (see below for a discussion for the origins of volume change during tensile testing).

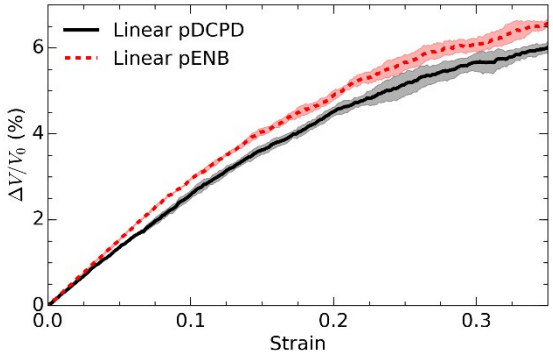

Figure S7. Change in volume of linear pDCPD and pENB during molecular dynamics simulations in the glassy state (150 K).

Investigation of Volume Change and Crazing in ROMP Tensile Specimens

Molecular simulations[8, 9] have suggested that the unusual toughness of ROMP polymers, when compared to epoxies of similar T_g, is due to the more energetically favorable formation of voids during strain in the non-polar ROMP polymers. To macroscopically investigate the propensity for nucleation and plastic growth of voids in these ROMP copolymers, the change in volume $\Delta V/V_0$ in quasi-static uniaxial tensile tests was estimated from the elongational strain ε_{zz} and transverse strain ε_{xx}, measured by digital image correlation as described in [10]:

$$\frac{\Delta V}{V_0} = (1 + \varepsilon_{zz})(1 + \varepsilon_{xx})^2 - 1 \quad \textbf{(S1)}$$

Representative tensile stress-strain curves and corresponding $\Delta V/V_0$ curves are plotted in Figure S8A and B for all formulations measured at room temperature. A similar plot for measurements at T_g-75°C is shown in Figure S9. Volume increase with elongational strain is similar for all formulations, with no systematic trend relative to M_c. The contributions to elongational strain from elasticity, voiding, and shear yielding can be estimated from the data in Figure S8A and B by [10-12]

$$\varepsilon_{Elastic} = \frac{\sigma}{E} \quad \text{(a)}$$

$$\varepsilon_{Void} = \frac{\Delta V}{V_0} - \frac{\sigma}{E}(1 - 2\nu) \quad \text{(b)}$$

$$\varepsilon_{Shear} = \varepsilon - (\varepsilon_{Elastic} + \varepsilon_{Void}) \quad \text{(c)} \quad \textbf{(S2)}$$

Strain components estimated according to Equations (S2)a-c are plotted in Figure S8C-E. This analysis reveals that shear yielding constitutes about 75% of large strain plastic deformation in this series of materials, with the remaining 25% due to voiding or crazing.

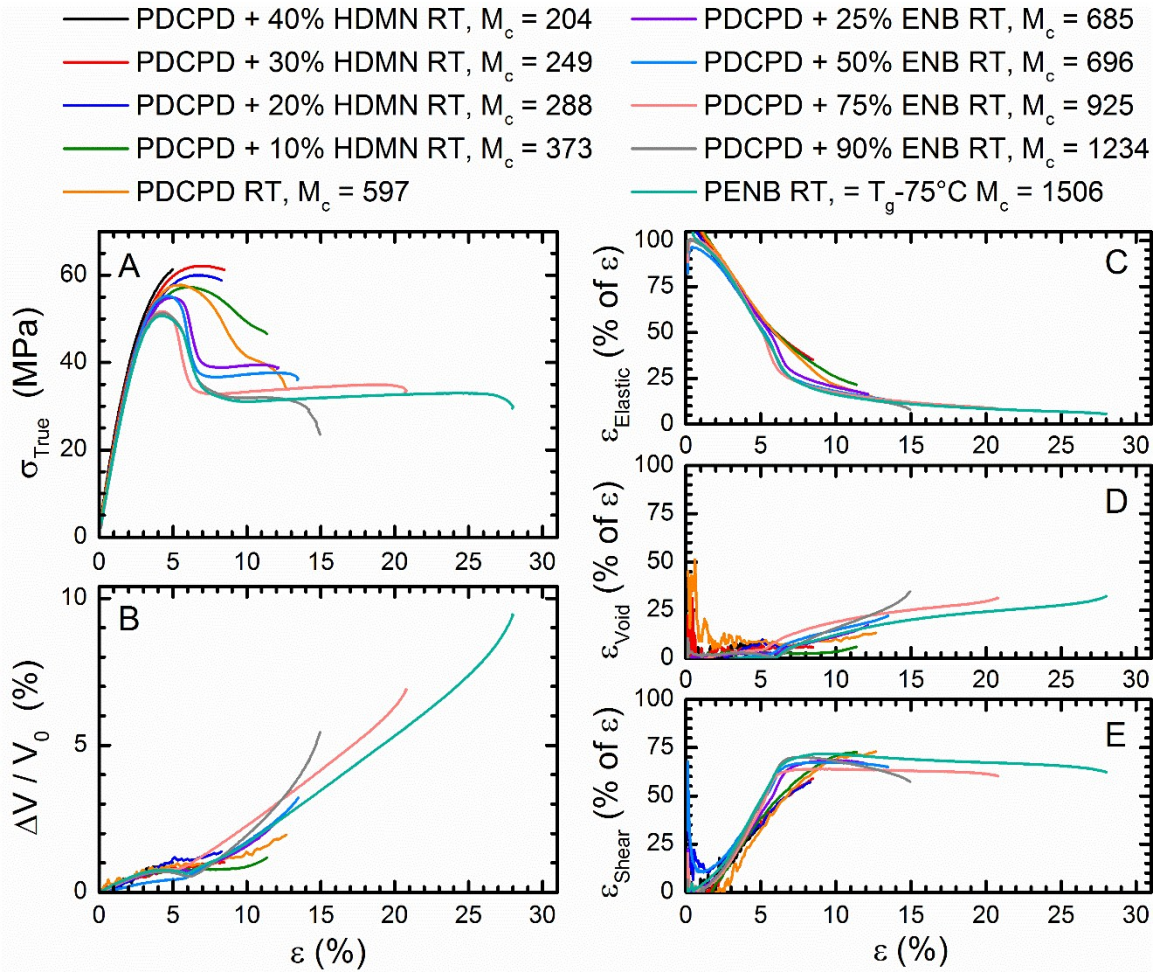

Figure S8. A) Representative tensile data at room temperature: (A) stress-strain curves, (B) change in volume $\Delta V/V_0$ estimated by equation (S1), (C-D) Percentage of strain due to (C) elastic deformation, (D) voiding, and (E) shear yielding, estimated by equations (S2).

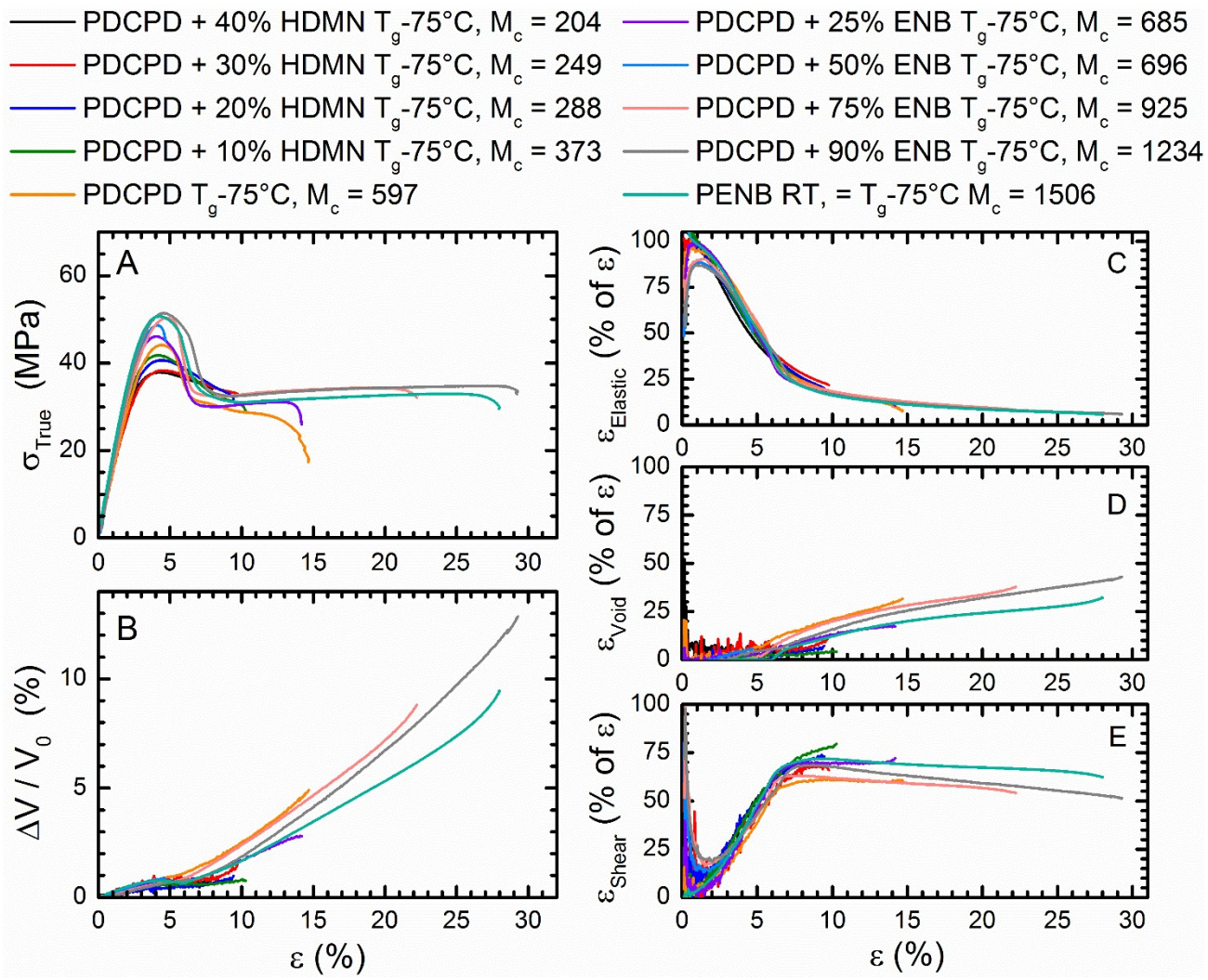

Figure S9. Representative tensile data at T_g-75°C: (A) stress-strain curves, (B) change in volume $\Delta V/V_0$ estimated by equation (S1), (C-D) Percentage of strain due to (C) elastic deformation, (D) voiding, and (E) shear yielding, estimated by equations (S2).

Figure S10 shows scanning electron microscopy (SEM) images of front faces of failed quasi-static tensile specimens of the ENB/DCPD copolymer series, taken from the necked region where plastic strain is greatest. These regions feature microcracks oriented perpendicular to the tensile stress. With decreasing M_c, the surface density of microcracks decreases significantly, and arrays of microcracks tend to align at 45 degree angles to the stress. These trends suggest a transition from a greater proportion of shear banding at lower M_c to a greater extent of crazing at higher M_c[13], although an increased volume change due to crazing is not observed for higher M_c samples in Figures S8 and S9.

Although crazing can occur for crosslinked polymer networks of sufficiently low crosslink density, the systems studied here have a higher density of entanglements ($4x10^{26}$ m^{-3} for pENB) and crosslinks ($1x10^{27}$ m^{-3} for pDCPD) than typically observed for polymers that craze readily[13]. Nevertheless, high magnification images in the right column of Figure S10 show a nodular structure on the surface of the microcracks, which has been associated with ruptured craze fibrils[14 15]. This nodular texture is similar over

the range of M_c from 600-1500, with a primary node size less than 100 nm, consistent with craze fibril diameters observed for other systems using SEM and TEM[13, 14]. The microcracks observed here are several orders of magnitude larger than nanovoids predicted to occur for pDCPD and pPENB in [8, 9] and the present work. Crazes are thought to nucleate as micro or nanovoids[13], but the craze widening stress is generally considered to govern the competition between macroscopic deformation via crazing or shear. Rottler and Robbins[16] predicted that initial cavitation requires a state of triaxial tension, but note that craze nucleation is often defect-dominated in real systems. The role of nanovoiding in craze nucleation and macroscopic failure of polymer networks should thus be a subject of future research.

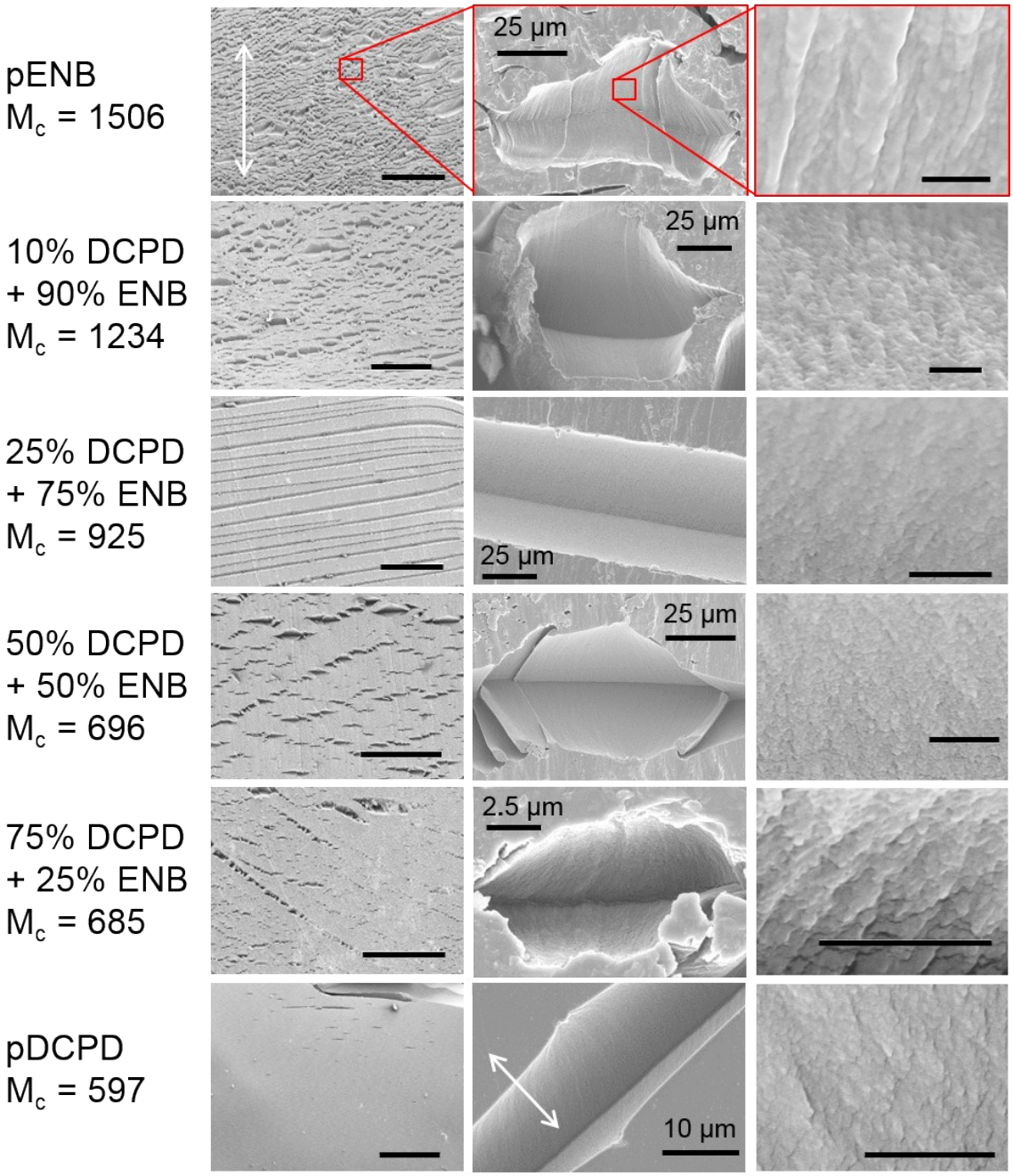

Figure S10. Front faces of failed tensile specimens of series ENB/DCPD copolymers at varying magnification. Scale bars are 500 µm (left column) and 1 µm (right column). Arrows indicate tensile direction (vertical for all images unless otherwise noted).

References

1. X. Sheng, M. R. Kessler and J. K. Lee, *Journal of Thermal Analysis and Calorimetry*, 2007, **89**, 459-464.
2. S. Deng, L. Ye and K. Friedrich, *Journal of Materials Science*, 2007, **42**, 2766-2774.
3. J. Ma, M.-S. Mo, X.-S. Du, P. Rosso, K. Friedrich and H.-C. Kuan, *Polymer*, 2008, **49**, 3510-3523.
4. T. H. Hsieh, A. J. Kinloch, K. Masania, A. C. Taylor and S. Sprenger, *Polymer*, 2010, **51**, 6284-6294.
5. E. D. Crawford and A. J. Lesser, *Polymer Engineering and Science*, 1999, **39**, 385-392.
6. L. Plangsangmas, J. J. Mecholsky and A. B. Brennan, *Journal of Applied Polymer Science*, 1999, **72**, 257-268.
7. E. D. Bain, D. B. Knorr, A. D. Richardson, K. A. Masser, J. Yu and J. L. Lenhart, *Journal of Materials Science*, 2016, **51**, 2347-2370.
8. R. M. Elder, D. B. Knorr, J. W. Andzelm, J. L. Lenhart and T. W. Sirk, *Soft Matter*, 2016, **12**, 4418-4434.
9. D. B. Knorr Jr, K. A. Masser, R. M. Elder, T. W. Sirk, M. D. Hindenlang, J. H. Yu, A. D. Richardson, S. E. Boyd, W. A. Spurgeon and J. L. Lenhart, *Composites Science and Technology*, 2015, **114**, 17-25.
10. E. D. Bain, R. A. Mrozek and J. L. Lenhart, *Mechanics of Materials*, 2017, **104**, 1-12.
11. D. Heikens, S. D. Sjoerdsma and W. J. Coumans, *J Mater Sci*, 1981, **16**, 429-432.
12. J. M. Gloaguen and J. M. Lefebvre, *Polymer*, 2001, **42**, 5841-5847.
13. E. J. Kramer and L. L. Berger, *Advances in Polymer Science*, 1990, **91/92**, 1-68.
14. P. Beahan, M. Bevis and D. Hull, *Proceedings of the Royal Society of London. A. Mathematical and Physical Sciences*, 1975, **343**, 525-535.
15. B. D. Lauterwasser and E. J. Kramer, *Philosophical Magazine A*, 1979, **39**, 469-495.
16. J. Rottler and M. O. Robbins, *Phys Rev E Stat Nonlin Soft Matter Phys*, 2003, **68**, 011801.